EPJ Photovoltaics **11**, 6 (2020)

https://doi.org/10.1051/epjpv/2020003

Available online at:
www.epj-pv.org

REGULAR ARTICLE OPEN ACCESS

Optimized amorphous silicon nitride layers for the front side passivation of c-Si PERC solar cells

Asmaa Mohamed Okasha Mohamed Okasha[1,2,*], Bishal Kafle[1], Benjamin Torda[1], Christopher Teßmann[1], and Marc Hofmann[1]

[1] Fraunhofer Institute for Solar Energy Systems ISE, Heidenhofstraße 2, 79110 Freiburg, Germany
[2] Department of Physics, Faculty of Science, Menoufia University, Menoufia, Egypt

Received: 23 August 2019 / Received in final form: 6 March 2020 / Accepted: 3 April 2020

Abstract. Plasma-enhanced chemical vapour deposition (PECVD) SiN_x is the typical choice as anti-reflection coating (ARC) for Silicon based solar cells. However, there still exists a room for improvement in passivation quality of SiN_x while maintaining good optics for the front side of a solar cell. In this paper, we studied in detail the optical and electrical properties of SiN_x layers by varying the chamber pressure and substrate temperature in an industrially used inline PECVD tool. Both the optical as well as electrical properties of SiN_x layers were found to be significantly influenced by the chamber pressure and substrate temperature. A trade-off between excellent optics and low surface recombination is observed with an increase in chamber pressure, whereas higher substrate temperature generally led to better passivation quality. The Si-H bond density, which is expected to directly influence the quality of surface passivation, increased at high pressure and at low substrate temperature. Based on our investigations, a good compromise between optics and surface passivation is struck to prepare optimized SiN_x layers and apply them as passivation layers for the front side of passivated emitter and rear cell (PERC) solar cells. The best solar cells show high short-circuit current density (j_{SC}) of 39.9 mA/cm^2 corresponding to the SiN_x layers with low parasitic absorption, good antireflection property, and excellent passivation of the surface and bulk silicon. The current-voltage (I-V) results are found to be in agreement with internal quantum efficiency (IQE) measurements of the solar cells.

Keywords: PERC cells / PECVD / passivation

1 Introduction

Amorphous hydrogenated silicon nitride (a-SiN_x:H) prepared by Plasma-Enhanced Chemical Vapour Deposition (PECVD), is the most common type of anti-reflective coating (ARC) used in crystalline silicon based solar cells. PECVD SiN_x layers have an optimal refractive index and low parasitic absorption coefficient and thereby augment the surface texture of silicon substrate, increasing the photocurrent generation of the solar cell. Furthermore, PECVD leads to a high amount of hydrogen species incorporated in the SiN_x layer, which can passivate bulk and surface defects during deposition or by diffusing to the interface after thermal treatment [1,2]. Although a-SiN_x:H deposited by PECVD is known to exhibit positive fixed charges [3,4], chemical passivation of defects by H-species is considered to be the major driving force behind excellent surface passivation quality, regardless of the substrate doping. For example, Richter et al. reached surface recombination velocity (SRV) of 64 cm.s^{-1} for 70 nm a-SiN_x:H on 1 Ω.cm *n*-type Si using PECVD with microwave (MW) induced plasma excitation [5]. Mäckel et al. used a mixture of $SiH_4/N_2/H_2$ to deposit a-SiN_x:H layers that showed good passivation performance. After forming gas annealing and rapid thermal firing, Mäckel et al. attributed the change in lifetime to the change in Si-H bond density [6]. They achieved SRV of 4–6 cm.s^{-1}, which correlates to an effective minority charge carrier lifetime (τ_{eff}) of 1200 µs on 1.25 Ω.cm *p*-type Si.

Wan et al. studied the effect of deposition parameters on the layer properties of a-SiN_x:H deposited in a combined MW/radio frequency PECVD reactor [7]. Soppe et al. deposited layers with refractive indices of 2.2 and achieved a reasonable passivation quality (SRV < 30 cm.s^{-1}) on *p*-type FZ wafers after thermal annealing [8]. Nagel et al. reported on a-SiN_x:H layers with refractive indices of 2.1 that served as good passivation layers for n$^+$ p silicon solar cells [9].

* e-mail: asmaa.mohamed.okasha.mohamed.okasha@ise.fraunhofer.de

In this study, we report on the effects of varying the PECVD deposition parameters on a-SiN_x:H layer properties with the aim of reaching high light transmission and good passivation for the front side of Passivated Emitter and Rear Cell (PERC) architecture. We show a correlation between the deposition parameters, antireflection property, bond densities and passivation quality of the layers. Spectroscopic ellipsometry and Fourier transform infrared spectroscopy (FTIR) are mainly used to gain insight on the influence of parameter variation on optics and structural properties of the deposited layer, respectively. Finally, PERC solar cells are fabricated with PECVD SiN_x deposited using selected parameter combinations. The solar cells are characterized using current-voltage (I-V) and quantum efficiency (QE) measurements and the results are discussed to correlate the electrical properties of solar cells with optical and structural properties of the deposited SiN_x layers.

2 Methods

2.1 Preparation of a-SiN_x:H

Shiny etched, p-type monocrystalline float zone (FZ) silicon substrates with a specific resistivity of 10 Ω.cm and thickness of 250 µm were used for ellipsometry and FTIR measurements. The FZ wafers underwent wet chemical cleaning with hot HNO_3 and a subsequent dip in diluted HF. The deposition of a-SiN_x:H layers was performed using a Meyer Burger MAiA PECVD inline reactor employing a linear microwave (MW) plasma source driven at 2.45 GHz. A silane (SiH_4) flux of 200 sccm and an ammonia (NH_3) flux of 600 sccm were used, and this gas ratio was kept constant throughout the experiment. Silane was fed to the plasma chamber from inlets on the sides close to the wafers, whereas ammonia was fed into the chamber via gas inlets far from the wafers and dissociates in the microwave region as can be seen in the schematic in Figure 1.

The deposition took place with the samples continuously transported underneath the linear plasma source. The samples were deposited at substrate temperatures of 300 °C and 400 °C and a variation of chamber pressure in the range of 0.10–0.30 mbar was performed. The deposited samples then received a fast firing process at a set peak temperature of 820 °C for about 3 seconds. Infrared absorption spectra were measured using a VERTEX 80 v spectrometer (Bruker) from 400 to 4000 cm^{-1}. Ellipsometry measurements were performed at three incident angles using M-2000 spectroscopic ellipsometer (J. A. Woollam Co).

This tool measures the time-dependent complex functions associated with Psi and Delta, and angles, as such, (or rather their trigonometric functions – cos 2 Psi and cos Delta) are obtained from it in a rather complex calculation procedure using Fourier analysis [10]. IV measurements were performed at standard test conditions using a solar cell simulator with a reference cell that is calibrated at Fraunhofer ISE Callab. Quantum efficiency of the solar cells was measured using a LOANA tool (PV Tools).

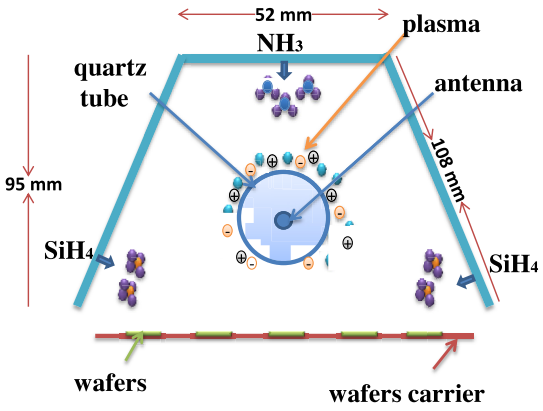

Fig. 1. Schematic cross-section diagram of the PECVD tool.

The formation of the a-SiN_x:H layers can be explained by the dissociation of ammonia and silane [7]. The incorporation of the SiH_x and NH_x radicals control the resultant amount of Si-H and N-H bonds, which depend on the substrate temperature. At an elevated temperature, a densification of the film occurs due to cross-linking, in which Si–H and N–H breaks and Si–N forms [7]:

$$\mathrm{Si{-}H + N{-}H \rightarrow Si{-}N + H_2}. \quad (1)$$

This mechanism explains the decrease in hydrogen, Si-H and N-H bonds with increasing substrate temperature. Breaking of both of these bonds would lead to dangling bonds and subsequently to the enhanced formation of Si-N bonds, resulting in denser layers. For high concentrations of NH_x radicals in the chamber, the breaking of Si-H bonds is the limiting factor for the formation of Si-N bonds.

2.2 Solar cell processing

Large area (156 × 156 mm^2) 2.6 Ω.cm p-type CZ precursors with alkaline texture, a homogeneous emitter and rear-side passivation were supplied to Fraunhofer ISE by Solar World Innovations GmbH. Test groups were passivated on the front side by a-SiN_x:H layers deposited using different deposition process parameters. All the samples were then processed together to create industrial PERC-type architectures and then characterized.

3 Results

3.1 Ellipsometery analysis

WVASE program (J. A. Woolam Co.) was used to analyse the results from ellipsometer measurements and to determine the optical constants (n and k). We used a Tauc Lorentz model [11] for fitting the results as it is applicable for amorphous materials with low absorption in the visible and-/or UV region of the spectrum. The optical constants for these layers, refractive index (n at 632 nm) and the extinction coefficient (k at 300 nm) are shown in Figures 2 and 3, respectively.

At low chamber pressures, the expansion of the plasma is likely to lead to the activation of both SiH_4 and NH_3

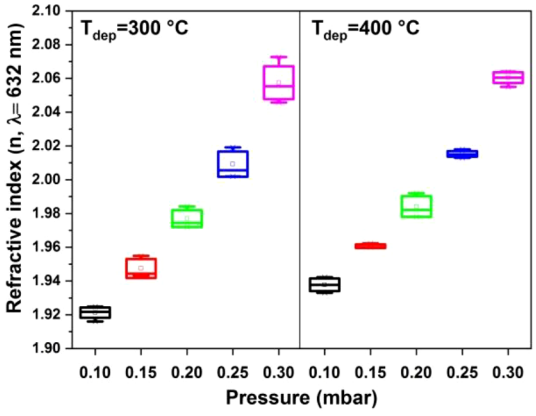

Fig. 2. Refractive index of a-SiN_x:H layers deposited at different pressures and temperatures.

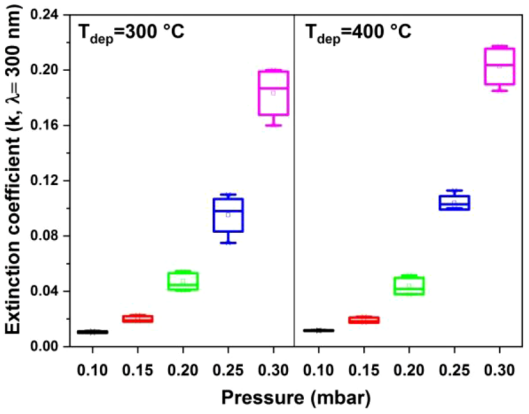

Fig. 3. Extinction coefficient of a-SiN_x:H layers deposited at different pressures and temperatures.

species; however, a higher dissociation rate of NH_3 in the plasma is expected to occur. Hence, in such conditions, NH_3 is likely to have higher contribution in the layer formation, which leads to the formation of SiN_x layers with lower density and higher nitrogen incorporation. Increasing the chamber pressure leads to plasma confinement, which consequently decreases the mean free path length of the species in the plasma and the corresponding likelihood of a lower fraction of dissociated precursor molecules. In such a scenario, a fraction of NH_3 molecules is expected to reach to the substrate without dissociation. Meanwhile, although SiH_4 is also likely to reach the substrate without dissociations, the high reactivity of SiH_4 molecules is expected to form a Si-rich SiN_x. NH_3 dissociation near the quartz tube was previously explained by Soppe et al. as in equation (2) [8]

$$NH_3 + e^- \rightarrow NH_2 + H + e^-. \quad (2)$$

The most common reactions at the higher chamber pressure are [8]:

$$SiH_4 + NH_2^* \rightarrow SiH_3 + NH_3\uparrow \quad (3)$$

$$SiH_4 + H \rightarrow SiH_3 + H_2\uparrow \quad (4)$$

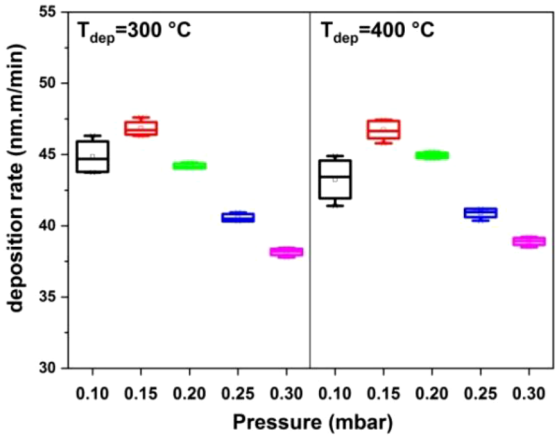

Fig. 4. Deposition rate as a function of chamber pressure and substrate temperature. For higher pressures, a decrease of the deposition rate occurs at all temperatures.

where the sign ↑ refers to gas molecule formation. Hence, Si-rich a-SiN_x:H layers are formed at high chamber pressure. Such layers have higher parasitic absorption of incident light and therefore should be avoided for their application as optimal anti-reflective layers in solar cells.

At low chamber pressure, dissociation of SiH_4 occurs more readily. The dissociation of SiH_4 can be explained as in equations (5) and (6) [8]:

$$SiH_4 + e^- \rightarrow SiH_3 + H + e^- \quad (5)$$

$$SiH_4 + e^- \rightarrow SiH_2 + 2H + e^-. \quad (6)$$

3.2 Deposition rate

Using ellipsometery, we measured the thickness of the layers to calculate the deposition rate of various process parameter combinations. Figure 4 shows the dependence of the deposition rate of a-SiN_x:H on pressure and temperature.

Above a chamber pressure of 0.15 mbar, the deposition rate decreases with increasing pressure. This behaviour, observed at all substrate temperatures, potentially arises due to the plasma confinement. At a low pressure of 0.10 mbar, a different behaviour was observed, as seen in the lower deposition rate in comparison to the deposition rate at 0.15 mbar. This is possibly due to a larger concentration of active species that could form due to the expansion of the plasma and the resulting increase in collisions between plasma species.

3.3 Etching rate

Etching of a-SiN_x:H in 1% hydrofluoric acid (HF) is previously shown to correlate to the density of the layers and also to the bulk passivation quality [12]. The etching of a-SiN_x:H in HF is attributed to the breaking of Si-N bonds and simultaneous replacement by Si-F bonds [13]. This method is also employed in the present study to compare

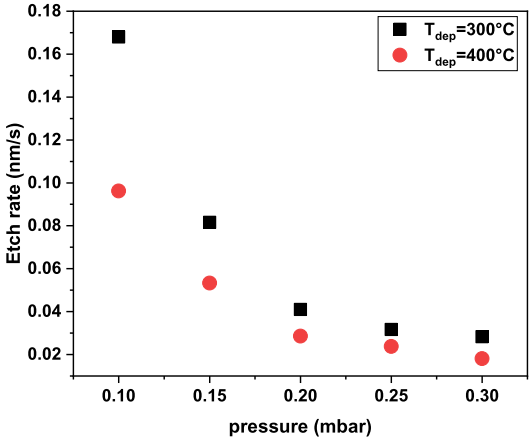

Fig. 5. Etching rate in 1% HF of layers deposited at different pressures and temperatures.

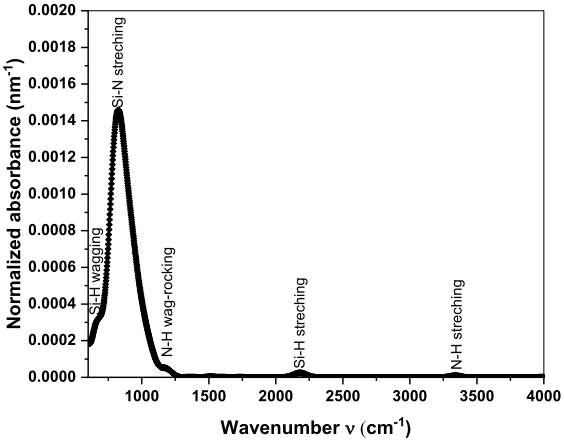

Fig. 6. Normalized absorbance (absorbance divided by thickness) versus wavenumber for as-deposited layers.

the density of layers formed at different chamber pressures. The deposited layers were etched for different durations, and thickness was measured in between the etching steps by spectroscopic ellipsometry. Figure 5 plots the etching rate of a-SiN_x:H layers deposited at different values of chamber pressure and substrate temperature. Regardless of the substrate temperature, the layers prepared at higher chamber pressure showed higher resistance to HF etching. This can be attributed to the formation of Si-rich layers at higher pressure [12] and faster etching of Si-N rich layers [14]. Si-rich layers often have better passivation quality [12]. The effect of temperature is clear in the layers deposited at low temperature 300 °C, which have higher hydrogen content and are expected to exhibit high porosity. Layers with low density will have higher etching rates, which was the case for the layers deposited at 300 °C compared to the layers deposited at 400 °C.

3.4 FTIR analysis

Fourier transform infrared spectroscopy (FTIR) measurements were performed in order to obtain details about the structure of the deposited a-SiN_x:H films. An example IR absorbance spectrum of an a-SiN_x:H film after subtracting the background, baseline correction and normalizing the absorbance by the measured thickness is shown in Figure 6.

Here, the following modes of vibrations can be observed: Si-N stretching mode around 832 cm^{-1} [15], N-H wagging-rocking mode around 1180 cm^{-1} [16], Si-H wagging mode around 640 cm^{-1} [15], Si-H stretching mode around 2180 cm^{-1} [15] and N-H stretching modes around 3340 cm^{-1} [15].

Using the FTIR data, the bond densities of N-H and Si-H bonds can be calculated by multiplying the Gaussian-fitted area of the peak with the calibration factor k as per [17]:

$$A_{X-Y} = k_{X-Y} \int_{400}^{4000} \alpha(\nu) d\nu \qquad (7)$$

where A_{X-Y} is the bond density of X-Y bond, k is the calibration factor.

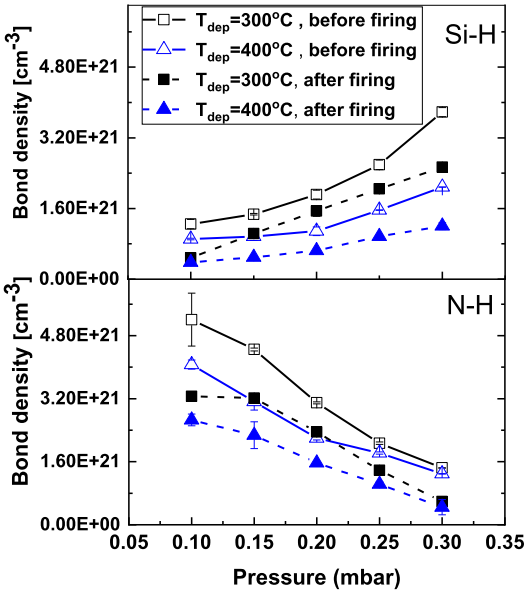

Fig. 7. The Si-H (top) and N-H (bottom) bond densities for a-SiN_x:H before and after fast firing.

The k values used here are:
$k_{Si-H} = 5.9\times10^{16}$ cm^{-1} and $k_{N-H} = 8.2\times10^{16}$ cm^{-1} [17]. The bond densities for different deposition parameters are plotted for the cases before and after the fast-firing process in Figure 7.

Figure 7 suggests that, in general for all parameter combinations, the Si-H and N-H bond densities measured after the fast firing process are lower than those measured just after the deposition process. The decrease in the Si-H and N-H bond densities in the layer after the firing process can be attributed to the effusion of H-species from the SiN_x layer due to the thermal budget applied by the fast-firing step [18]. Additionally, in-diffusion of H species into the Si-SiN_x interface is reported to occur, which is the basis for chemical passivation of the surface dangling bonds [7]. Both Si-H bond density and Si content increase

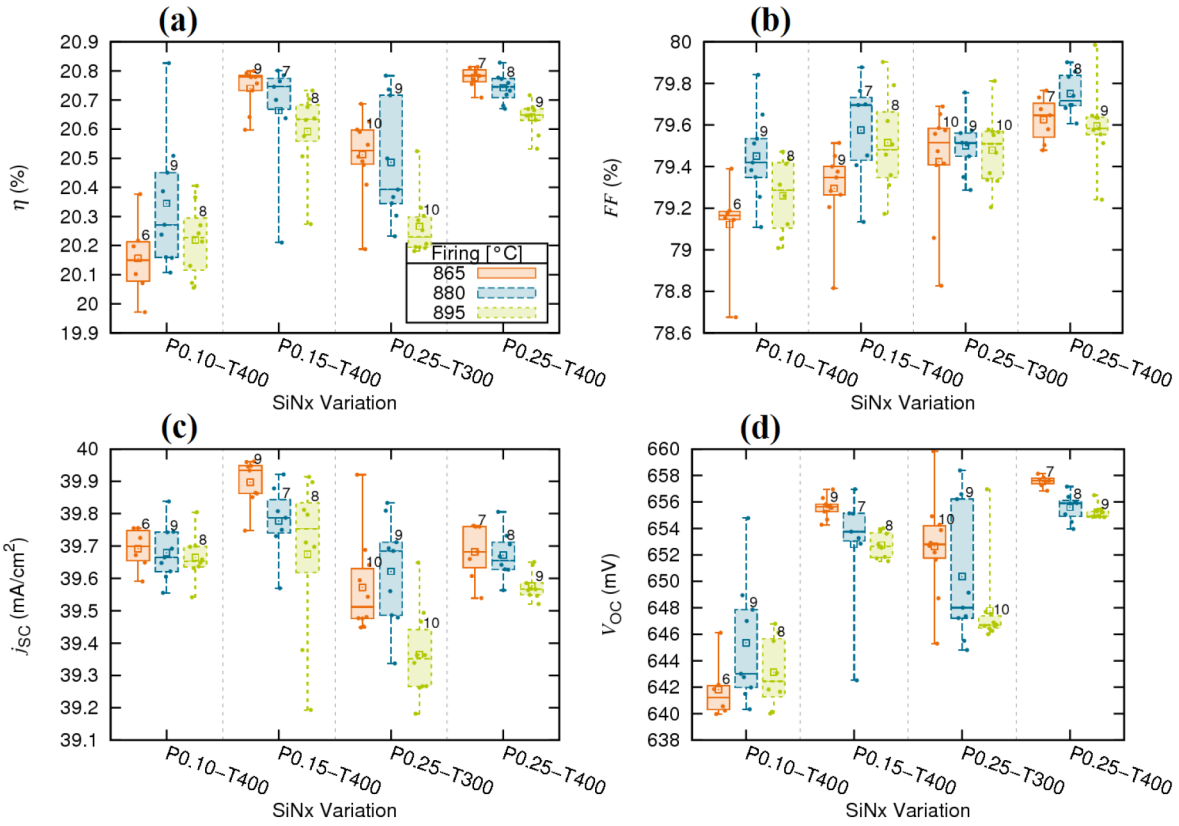

Fig. 8. I-V data for PERC-type solar cells with different front-side passivation schemes. Cell area is 242.84 cm^2 and all cells feature solder pads. In x-axis legend, P stands for chamber pressure and T stands for the deposition temperature.

with increasing pressure, potentially due to plasma confinement. This observation correlates very well with the measured optical properties in Figures 2 and 3, where an increase in the chamber pressure resulted in higher values of n and k.

Additionally, lowering the substrate temperature increased the Si-H bond density in a-SiN$_x$:H layers. In fact, the higher substrate temperature (400 °C) led to the lowest hydrogen content in a-SiN$_x$:H. A potential explanation is that there was an increase in effusion of hydrogen species from the layers due to the breaking of weak Si-H and N-H bonds at higher temperature [17].

3.5 Solar cell results

Passivated emitter and rear solar cells were fabricated to investigate the applicability of the developed layers on the target device. The measured parameters of the passivated emitter and rear cells (PERC) after applying selected a-SiN$_x$:H layers as front side anti-reflection coatings is shown in Figure 8. It can be observed that a-SiN$_x$:H layers deposited using different parameter combinations show different optical and passivation properties for the front side of PERC cells. Explanation of these results, discussing the influence of chamber pressure and substrate temperature on solar cell characteristics, is presented in the following sections.

3.5.1 Dependence on pressure

For a-SiN$_x$:H layers prepared at different chamber pressure (0.10, 0.15 and 0.25 mbar) whereas maintaining a higher temperature (400 °C), layers deposited at 0.10 mbar exhibited relatively low passivation quality. Worse passivation resulted in a lower open-circuit voltage, V_{OC}, potentially due to high layer porosity compared to other layers deposited at higher pressures. The layers deposited at the lowest pressure are not optimally applicable as an ARC, since the refractive index, at $n = 1.94$, is too low [9]. Layers deposited at 0.15 mbar ($n \approx 1.97$) and 0.25 mbar ($n \approx 2.06$) are better suited to the target application (higher n values are better for the overall module optics) and showed lower nitrogen content, as per the estimation of the N-H bond density from the FTIR spectra.

The reduction of the short-circuit current density, j_{SC}, from 0.15 mbar to 0.25 mbar can be attributed to an increase in the extinction coefficient k. The increase of j_{SC} between the two process pressures 0.10 mbar and 0.15 mbar can be attributed to the increase in passivation quality as it also led to a simultaneous increase in V_{OC} value (see Fig. 8d).

The fill factor is observed to increase with an increasing value of process pressure. One hypothesis here is that the firing process, including the silver paste composition, was optimized for higher density a-SiN$_x$:H layers like P0.25-T400 (pressure of 0.25 mbar and a temperature of 400 °C).

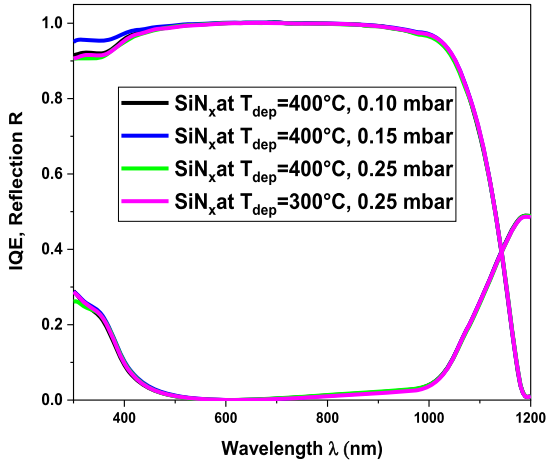

Fig. 9. Internal quantum efficiency (IQE) of the applied a-SiN_x:H for front side passivation of PERC-type solar cells.

3.5.2 Dependence on temperature

For the layers deposited at different temperatures (300 °C and 400 °C) and the same pressure (0.25 mbar), we can see that the layers at higher temperature showed the best performance in terms of j_{SC}. This is in accordance with the etching rate results, which showed that layers deposited at higher temperature show less porosity and contain enough hydrogen (from Si-H bond density), which is widely reported to be necessary for good passivation.

For the best solar cell, an open-circuit voltage (V_{OC}) of 660 mV and short-circuit current density (j_{SC}) of 40 mA/cm^2 with a cell efficiency (η) of 20.9% was reached. A higher V_{OC} is attributed to an improved front-side passivation achieved by implementing the best PECVD a-SiN_x:H layers.

In the same way, we can explain the results for Internal Quantum Efficiency (IQE) and reflection (R) that are shown in Figure 9. A significant improvement was found for the parameter set including the deposition temperature of 400 °C and a pressure of 0.15 mbar.

This is due to low reflection, high homogeneity and low porosity (as shown in Fig. 5 for the etching rate) of the deposited layer compared to that deposited at 0.10 mbar. Additionally, there was an increase in transparency (lower k values) than for the layers deposited at higher pressure. For the layers deposited at 0.15 mbar, there was also an improvement in j_{SC}.

The layers deposited at different temperatures, but at the same pressure, showed slightly better performance in the IQE for layers prepared at low temperature (300 °C). This may be due to the lower absorption (k values) for these layers than those prepared at 400 °C.

The bulk and the rear side passivation are comparable for all solar cells.

4 Conclusion

Amorphous hydrogenated silicon nitride (a-SiN_x:H) layers prepared by PECVD showed a dependence on both the deposition pressure and temperature. Higher pressure resulted in Si-rich layers, probably due to plasma confinement leading to low porosity. These layers also had good passivation properties. Layers deposited at low temperature showed higher hydrogen content, with higher porosity and etching rates. The firing process resulted in lower hydrogen content due to the effusion of hydrogen out of the layers and concurrent diffusion of hydrogen to the silicon-silicon nitride interface. Hydrogen diffusion would passivate dangling bonds and improve the layers' electrical properties. Higher IQE was found for layers deposited at the low pressure of 0.15 mbar, which also exhibited low light absorption. These results matched the layers' optical properties and the trend observed for j_{SC}.

The authors would like to thank the German federal ministry for economic affairs and energy for the financial support of this work under the contract number 0324171. B. A. M. O. M. Okasha thanks the Egyptian government for the funding within the scope of her dissertation.

Author contribution statement

All authors have contributed to the writing of the manuscript. More precisely, Asmaa Okasha and Bishal Kafle prepared the cells and coordinated the manuscript preparation. Benjamin Torda did the measurements and analysis for ellipsometer. Christopher Teßmann did the IV analysis. Marc Hofmann created the plan for process parameter variation in collaboration with Asmaa Okasha, and supervised the work.

References

1. R.S. Bonilla, B. Hoex, P. Hamer, P.R. Wilshaw, Phys. Status Solidi A **214**, 1700293 (2017)
2. J-F. Lelièvre, E. Fourmond, A. Kaminski, O. Palais, D. Ballutaud, M. Lemiti, Sol. Energy Mater. Sol. Cells **93**, 1281 (2009)
3. A.G. Aberle, Sol. Energy Mater. Sol. Cells **65**, 239 (2001)
4. W.L. Warren, C.H. Seager, J. Kanicki, M.S. Crowder, E. Sigari, J. Appl. Phys. **77**, 5730 (1995)
5. A. Richter, S.W. Glunz, F. Werner, J. Schmidt, A. Cuevas, Phys. Rev. B **86**, 187 (2012)
6. H. Mäckel, R. Lüdemann, J. Appl. Phys. **92**, 2602 (2002)
7. Y. Wan, K.R McIntosh, A.F Thomson, AIP Advances **3**, 32113 (2013)
8. W. Soppe, H. Rieffe, A. Weeber, Prog. Photovolt.: Res. Appl. **13**, 551 (2005)
9. H. Nagel, A.G. Aberle, R. Hezel, Prog. Photovolt.: Res. Appl. **7**, 245 (1999)
10. N.J. Podraza, G.E Jellison, *Encyclopedia of Spectroscopy and Spectrometry* (Elsevier, 2017)
11. D.N. Wright, E.S. Marstein, A. Holt, in *22nd European Photovotalic Conference and Exhibition, Milano, Italy, 2007*, p. 1651
12. H.F.W. Dekkers, S. De Wolf, G. Agostinelli, F. Duerinckx, G. Beaucarne, Sol. Energy Mater. Sol. Cells **90**, 3244 (2006)

13. D. Martin Knotter, T.J.J. Denteneer, Appl. Phys. Lett. **148**, F43 (2001)
14. M.S. Jeon, M. Dhamrin, T. Saitoh, K. Kamisako, in *IEEE 4th World Conference on Photovoltaic Energy Conference, Waikoloa, HI, USA, 2006*, p. 1425
15. F. Giorgis, C.F. Pirri, E. Tresso, Thin Solid Films **307**, 298 (1997)
16. E. Bustarret, M. Bensouda, M.C. Habrard, J.C. Bruyère, S. Poulin, S.C. Gujrathi, Phys. Rev. B **38**, 8171 (1988)
17. J.J. Mei, H. Chen, W.Z. Shen, H.F.W. Dekkers, J. Appl. Phys. **100**, 73516 (2006)
18. J. Hong, W.M.M. Kessels, W.J. Soppe, A.W. Weeber, W.M. Arnoldbik, M.C.M. Van de Sanden, J. Vacuum Sci. Technol. B **21**, 2123 (2003)

Cite this article as: Asmaa Mohamed Okasha Mohamed Okasha, Bishal Kafle, Benjamin Torda, Christopher Teßmann, Marc Hofmann, Optimized amorphous silicon nitride layers for the front side passivation of c-Si PERC solar cells, EPJ Photovoltaics **11**, 6 (2020)